Article

Variable Fractional-Order Equivalent Circuit Model for Lithium-Ion Battery via Chaotic Adaptive Fractional Particle Swarm Optimization Method

Deshun Wang [1,2,*], **Haikun Wei** [1], **Jinhua Xue** [2], **Fubao Wu** [3] **and António M. Lopes** [4]

1 School of Automation, Southeast University, Nanjing 210096, China
2 State Grid Shanghai Energy Interconnection Research Institute Co., Ltd., Shanghai 201203, China
3 Jiangsu Engineering Technology Research Center for Energy Storage Conversion and Application, China Electric Power Research Institute, Nanjing 210003, China
4 LAETA/INEGI, Faculty of Engineering, University of Porto, Rua Dr. Roberto Frias, 4200-465 Porto, Portugal
* Correspondence: wangdeshun@epri.sgcc.com.cn

Abstract: A variable fractional-order equivalent circuit model is proposed to accurately describe the dynamic characteristics of lithium-ion batteries (LIBs). Firstly, a fractional impedance model (FIM) is established, such that the fractional-order (FO) is a polynomial function of the LIB state of charge (*SOC*). Then, a chaotic adaptive fractional particle swarm optimization (CAFPSO) method is derived to identify the parameters of the FIM. Experiments reveal the reliability of the novel approach through the root-mean-squared error (RMSE) and the mean absolute error (MAE) of the LIB terminals voltage, yielding the values 8.99 mV and 4.56 mV, respectively. This translates into accuracy improvements of 22.5% and 34.4% for the particle swarm optimization (PSO) algorithm and 57.9% and 72.8% for the adaptive fractional particle swarm optimization (AFPSO) algorithm, respectively.

Keywords: FO equivalent circuit; parameters' identification; particle swarm optimization

1. Introduction

Under the background of more and more serious environmental problems and people's increasing concerns about environmental protection, developing and efficiently using renewable energy has become a key topic of research [1]. Wind and solar power generation are quite affected by natural environment conditions, such as weather and light changes, thus revealing volatility, intermittence and randomness. In order to mitigate these issues and to ensure stable and safe operation of the power grid, the development of effective energy storage systems is crucial [2].

Energy storage technologies can be grouped into electrochemical, physical and thermal categories. The electrochemical storage technology is the most widely adopted, and it relies on LIBs as one of the most mature storage media [3]. Indeed, LIBs are used in many equipments due to their characteristics, namely long service life, high energy density, low self-discharge rate, and small size. However, to ensure efficient, safe and stable operation, accurate state estimation is a crucial part of the LIBs management system. The premise to develop accurate state estimation methods is the availability of high-precision battery models [4].

For an efficient battery management system, a high-precision model that fits the dynamic characteristics of the LIB is very important. The so-called equivalent circuit model approach has been widely used, since it yields good precision, has simple structure and allows easy implementation [5]. The standard equivalent circuit model is made of a series of resistors, capacitors and inductors. However, the electrochemical impedance spectrum of a pure capacitor is inconsistent with the actual LIB dynamics. As such, equivalent circuit models were proposed that include FO components, denoted as constant phase

elements (CPE) [6], which have great influence on the model accuracy, and reveal a certain correlation with the *SOC* [7–11].

In addition to the model, the accuracy of the model parameters is critical [7,12,13]. Parameters' identification methods for LIBs have been widely addressed in the literature [14–16]. For instance, schemes based on PSO algorithms were discussed in references [9,17,18], while methods based on the recursive least squares technique were investigated in other works [19–21]. The parameters' identification method based on PSO has some limitations, such as population clustering caused by random initialization, lack of diversity, easy to fall in local optima, and slow convergence speed.

In this paper, an FIM that fits the LIB dynamics is set up based on the electrochemical impedance spectroscopy (EIS) technique. A new CAFPSO method is then proposed to accurately identify the FIM parameters. Chaotic initialization is used to improve the diversity of the initial population, and an adaptive fractional speed update law is adopted to increase the convergence rate of the algorithm and prevent it to fall into local optimal solutions [22]. The new CAFPSO significantly improves the accuracy of the FIM parameters' identification. The accuracy and effectiveness of the approach are assessed by means of the RMSE and the MAE of the LIB terminals voltage, which are equal to 8.99 mV and 4.56 mV, thus showing excellent accuracy.

The paper is structured into five sections. Section 2 introduces the basics of FO calculus and the FO capacitor device. Section 3 addresses the mathematical derivation of the LIBs FIM. Section 4 presents the CAFPSO and assesses the accuracy of the algorithm. Finally, Section 5 concludes the paper.

2. Preliminary Concepts

Basic Concepts of FO Calculus

The tools of calculus are commonly used for the mathematical description of dynamical systems. The FO calculus was put forward by Leibnitz in 1695 as an extension of the integer calculus to any real or complex orders. In recent decades, it has been realized that real physical systems, namely those including diffusion phenomena, hysteresis, hydrodynamics, and other characteristics, are better described by the tools of FO calculus than by standard integer-order models. For LIBs, the FO calculus is able to accurately describe their internal electrochemical dynamical characteristics.

Let us denote by D_t^α the derivative ($\alpha > 0$) or integral ($\alpha < 0$) operators of order $\alpha \in \mathbb{R}$, with respect to t, where t_0 is the initial time instant. Herein, we will consider $t_0 = 0$ and ($\alpha > 0$) and use the simplified notation D^α. Moreover, the Grünwald–Letnikov (GL) definition will be adopted. Therefore, given a function $x(t)$, we can write [23]:

$$D^\alpha x(t) = \lim_{\Delta T \to 0} \frac{1}{\Delta T^\alpha} \sum_{j=0}^{[t/\Delta T]} (-1)^j \binom{\alpha}{j} x(t - j\Delta T), \tag{1}$$

where ΔT represents the sampling period, the operator $[\cdot]$ stands for the integer part of the argument, and $\binom{\alpha}{j}$ corresponds to the generalization to real numbers of the Newton binomial, that is,

$$\binom{\alpha}{j} = \frac{\Gamma(\alpha + 1)}{\Gamma(j + 1) \cdot \Gamma(\alpha - j + 1)}, \tag{2}$$

with $\Gamma(\alpha)$ denoting the Gamma function:

$$\Gamma(\alpha) = \int_0^{+\infty} \xi^{\alpha - 1} e^{-\xi} d\xi. \tag{3}$$

In the state-space form, for a linear time-invariant FO system, we have:

$$\begin{cases} D^{\alpha}x(t) = Ax(t) + Bu(t) \\ \quad\quad y(t) = Cx(t) + Du(t) \end{cases} \tag{4}$$

3. The FO Modeling of LIBs

The EIS technique is often used to measure the AC impedance spectrum that characterizes the LIB dynamic response. Figure 1 (top) illustrates the impedance of a typical LIB using a Nyquist plot. The spectrum includes three main parts: (1) a low-frequency band in which the diffusion of solid-phase lithium-ions in the LIB electrodes occurs, (2) a middle-frequency band due to the charge transfer reaction and electrochemical double layer effect, and (3) a high-frequency band due to Ohmic resistance of inductive components. Integer-order equivalent circuit models use RC branches to model the mid-range band and ignore the characteristics of the low-frequency region. Moreover, as the EIS spectrum of an ideal capacitor is a semicircle in the Nyquist diagram, it is inconsistent with the ellipse-like curve actually observed. Thus, integer-order models cannot accurately describe the dynamic characteristics of LIBs. In this way, several works proposed using CPEs, instead of ideal capacitors, to establish an FIM that better describes the internal characteristics of LIBs. The impedance of a CPE is expressed as:

$$Z(s) = \frac{1}{Cs^{\alpha}}, \tag{5}$$

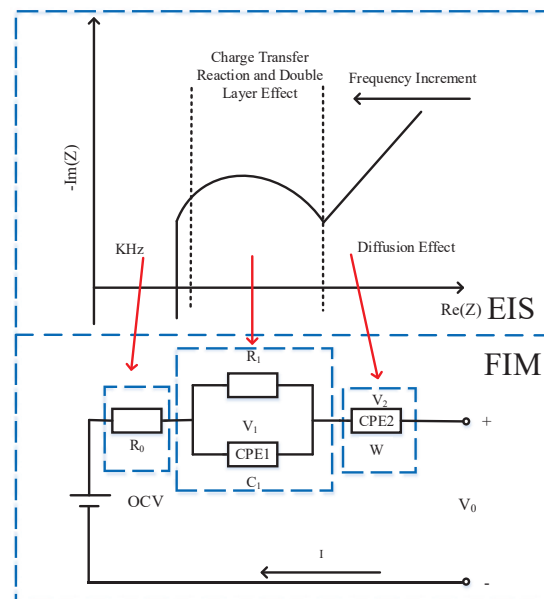where C is related to the element capacitance.

Figure 1. The EIS-FIM of a typical LIB.

Figure 1 (bottom) represents the FIM constructed to describe the dynamic characteristics of LIBs, where the circuit elements that model the regions (1)–(3) of the EIS are shown. In the model, the symbol I is the discharge current, OCV stands for the open circuit voltage, V_0 represents the battery terminals voltage, R_0 is the Ohmic internal resistance, C_1 and W are the CPEs, R_1 is the resistance on the RC parallel, V_1 corresponds to the voltage across the RC branch, and V_2 is the Warburg-like element voltage. Correspondingly, we use the W element to simulate the LIB characteristics in the low-frequency band, the RC parallel formed by a CPE and R_1 to model the characteristics in the medium-frequency band, and R_0 to simulate the high-frequency band.

As the curve representing the low-frequency band in the Nyquist diagram is always a $45°$ straight line, the FO of W is set to 0.5. The curve corresponding to the middle-frequency band changes with the *SOC* [24], so we express the FO α_1 of the CPE in the RC parallel as a polynomial function of the *SOC*, yielding:

$$\alpha_1(SOC) = \sum_{i=0}^{7} b_i SOC^i(t). \tag{6}$$

The *OCV-SOC* relationship is usually a nonlinear function, which we expressed as:

$$U_{OCV} = \sum_{i=0, i \neq 1}^{6} a_i SOC^i(t). \tag{7}$$

The FIM of the LIB can then be established based on the Kirchhoff's voltage and current laws, yielding:

$$
\begin{cases}
D^{\alpha_1(SOC)} x_1(t) = -\dfrac{V_1(t)}{R_1 C_1} + \dfrac{1}{C_1} u(t), \\[2mm]
D^{0.5} x_2(t) = \dfrac{1}{W} u(t), \\[2mm]
D^1 x_3(t) = -\dfrac{\eta}{Q_n} u(t), \\[2mm]
y(t) = OCV(x_3(t)) - x_1(t) - x_2(t) - R_0 u(t),
\end{cases}
\tag{8}
$$

where the function $u(t)$ stands for the input current, with a negative (positive) signal for charging (discharging), the vector $x(t) = [V_1(t), V_2(t), SOC(t)]^T$ is the state, and the function $y(t)$ denotes the output voltage. Moreover, the symbol Q_n represents the nominal capacity of the LIB, which is expressed in Ampere-hour (Ah), and the symbol η corresponds to the Coulomb efficiency.

Based on expression (4), the FO system given by (8) can be represented in the discrete-time, k, $(k \geq 1)$, $\alpha = [\alpha_1, 0.5, 1]$ as:

$$
\begin{cases}
x(k+1) = [(\Delta T)^\alpha A + \text{diag}(\alpha)I]x(k) \\[2mm]
\qquad - \displaystyle\sum_{j=2}^{L+1} (-1)^j \begin{pmatrix} \alpha \\ j \end{pmatrix} x(k+1-j) \\[2mm]
\qquad + (\Delta T)^\alpha B u(k), \\[2mm]
y(k) = OCV(x_3(k)) - x_1(k) - x_2(k) - R_0 u(k),
\end{cases}
\tag{9}
$$

where

$$(\Delta T)^\alpha = \text{diag}((\Delta T)^{\alpha_1(SOC)}, (\Delta T)^{0.5}, \Delta T), \tag{10}$$

$$\begin{pmatrix} \alpha \\ j \end{pmatrix} = \text{diag}\left(\begin{pmatrix} \alpha_1(SOC) \\ j \end{pmatrix}, \begin{pmatrix} 0.5 \\ j \end{pmatrix}, \begin{pmatrix} 1 \\ j \end{pmatrix} \right), \tag{11}$$

$$
A = \begin{bmatrix} -\frac{1}{R_1 C_1} & 0 & 0 \\ 0 & 0 & 0 \\ 0 & 0 & 0 \end{bmatrix}, B = \begin{bmatrix} \frac{1}{C_1} \\ \frac{1}{W} \\ -\frac{\eta}{Q_n} \end{bmatrix}. \tag{12}
$$

4. Parameters' Identification and FIM Validation

As seen in Figure 1, the FIM has unknown parameters, and obtaining their values is demanding. Therefore, it is crucial to accurately identify the LIM parameters by means of suitable methods. Herein, we propose a new CAFPSO method and assess its effectiveness.

The PSO is a simple and easy to implement algorithm inspired on birds' predation behavior. However, the traditional PSO has some drawbacks, such as the slow rate of convergence and it easy to fall into local optimal solutions, which leads to considerable errors in the identification process.

The initial position of the population is crucial in the performance of PSO. The logistic chaotic map can be adopted to generate an evenly distributed population, thus contributing to improve the performance of the algorithm. The logistic chaotic map is expressed as:

$$x_{k+1} = \mu x_k (1 - x_k), \tag{13}$$

where k is the iteration number, and $\mu \in (0, 4]$.

For logistic chaotic mapping, when $\mu = 4$, the system is chaotic, the distribution uniformity of the mapping reaches its peak, and the number of particle swarm is 300. Here, we adopt $\mu = 4$ and 300 iterations to generate the logistic chaotic sequence. The values are mapped to particle individuals to perform the initialization of the population, according to the formula:

$$\chi = \chi_{lb} + (\chi_{ub} - \chi_{lb})\chi_{k+1}, \tag{14}$$

where χ_{lb}, χ_{ub} are the upper and lower limits of each individual in each dimension, and χ is the mapped individual.

On the other hand, the AFPSO was introduced as a novel technique for controlling the convergence rate of the PSO algorithm that uses the concepts of FO calculus. It was shown that the FO directly influences the speed of convergence of the PSO. In order to avoid the algorithm falling into local optima and to improve search efficiency, an FO velocity adaptation law is adopted:

$$\begin{cases} D^q(v_i^{k+1}) = C_1 R_1 (P_{best_i}^k - \chi_i^k) + C_2 R_2 (G_{best_i}^k - \chi_i^k), \\ \chi_i^{k+1} = \chi_i^k + v_i^k, \end{cases} \tag{15}$$

Then, using the GL derivative (1) and $r = 4$ terms, one has:

$$\begin{cases} v_i^{k+1} = q v_i^{k+1} + \dfrac{1}{2}q(1-q)v_i^{k-1} \\ \qquad + \dfrac{1}{6}q(1-q)(2-q)v_i^{k-2} \\ \qquad + \dfrac{1}{24}q(1-q)(2-q)v_i^{k-3} \\ \qquad + C_1 R_1 (P_{best_i}^k - \chi_i^k) + C_2 R_2 (G_{best_i}^k - \chi_i^k), \\ \chi_i^{k+1} = \chi_i^k + v_i^k, \end{cases} \tag{16}$$

where q is adaptively updated by:

$$q = 0.8 - 0.5\frac{k}{K}, \tag{17}$$

with k denoting the current iteration and K denoting the total number of iterations. For good performance, $q \in [0.3, 0.8]$ is chosen.

The FIM parameters to be identified are encapsulated into the vector $\phi = [b_o, b_1, b_2, b_3, b_4, b_5, b_6, b_7, R_0, R_1, C_1, W]$. The parameters' identification objective is to find the parameters

values that minimize the fitness function, $f(\cdot)$, that represents the error between the measured and the predicted voltages, $V_0(k)$ and $\widehat{V}_0(k)$, respectively, meaning:

$$\min f(\cdot) = \min \sum_{k=1}^{M} [V_0(k) - \widehat{V}_0(k)]^2, \qquad (18)$$

where the symbol M denotes the total number of the sampling points. Figure 2 illustrates schematically the CAFPSO algorithm.
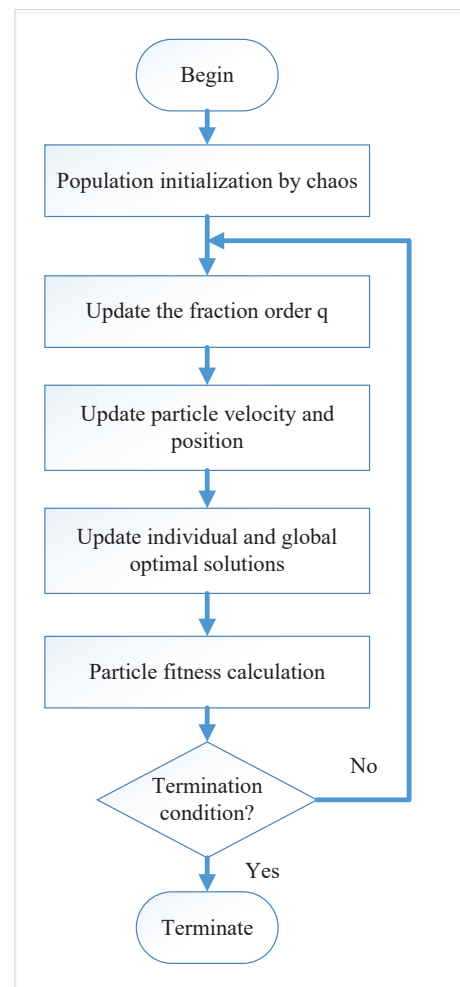

Figure 2. Schematic representations of the CAFPSO algorithm.

The RMSE and the MAE metrics are adopted to assess the accuracy of the CAFPSO, which are computed as:

$$RMSE \quad = \quad \sqrt{\frac{1}{M} \sum_{k=1}^{M} [V_0(k) - \widehat{V}_0(k)]^2}, \qquad (19)$$

$$MAE \quad = \quad \frac{1}{M} \sum_{k=1}^{M} \mid V_0(k) - \widehat{V}_0(k) \mid. \qquad (20)$$

For assessing the effectiveness of the method, we use data of voltage and current under LIB Dynamic Stress Test (DST) conditions. The nonlinear relationship between *OCV* and *SOC* was fitted by a 6th-order polynomial based on low-current *OCV* test data. Table 1 summarizes the identified polynomial coefficients and Table 2 lists the parameters' values obtained with the new CAFPSO. In order check the effectiveness of the CAFPSO, we compare the voltages

estimated when using the parameters identified by the CAFPSO, the PSO and the AFPSO. Figures 3 and 4 depict the obtained voltage and the voltage absolute error for 25 °C. From Figure 3, we verify that the parameters identified by the CAFPSO yield better results than the ones identified by both the PSO and AFPSO alternatives. From Figure 4 and Table 3, we verify that the RMSE by the CAFPSO, PSO and AFPSO are 8.99 mV, 11.6 mV and 21.4 mV, respectively, while the MAE yields 4.56 mV, 6.95 mV and 16.8 mV. Therefore, the identified parameters lead to good accuracy, and the proposed FIM and CAFPSO are reliable.

Table 1. The identified coefficients of the *OCV-SOC* polynomial.

a_0	a_1	a_2	a_3	a_4	a_5	a_6
3.159	2.499	−9.197	17.860	−16.717	8.259	−1.816

Table 2. The result of the parameters' identification with the CAFPSO.

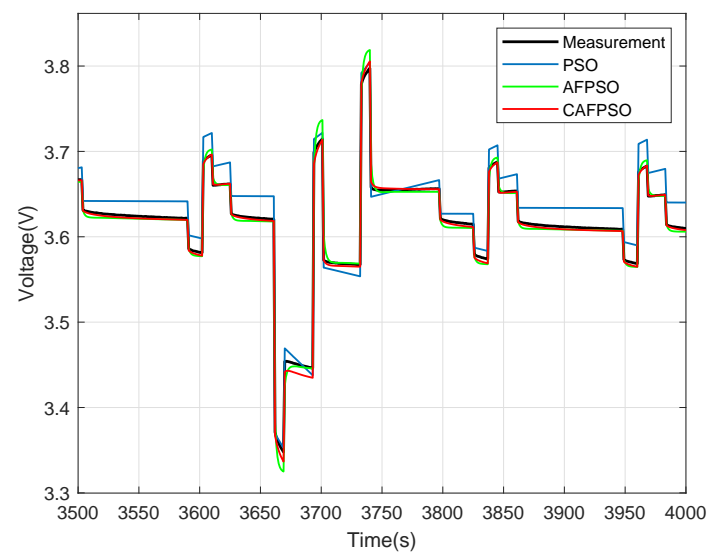| b_0	b_1	b_2	b_3	b_4	b_5
0.9932	−1.7075	1.6735	−0.4257	−1.2296	3.0521
b_6	b_7	R_0	R_1	C_1	W
−2.2960	0.6695	0.0721	0.3685	1977	976.211

Figure 3. The LIB terminals measured and estimated voltages by the CAFPSO, PSO and AFPSO.

Table 3. The values of the RMSE and MAE metrics of the LIB terminals voltage with the parameters' identification by the CAFPSO, PSO and AFPSO.

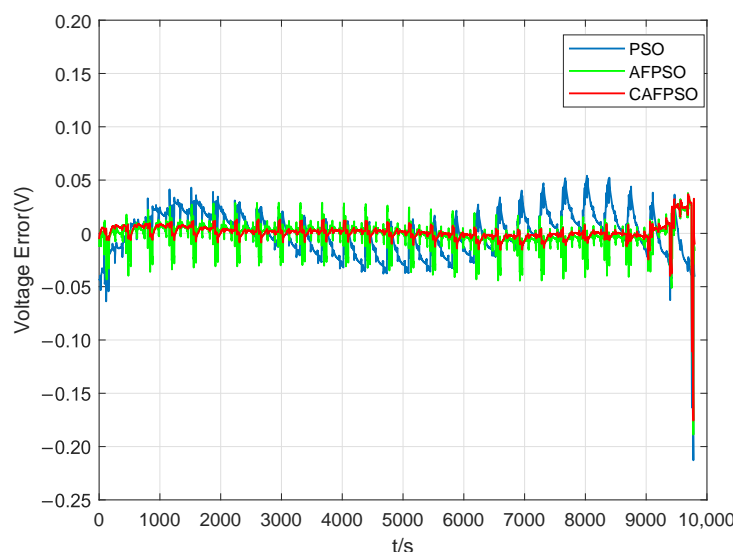|	PSO	AFPSO	CAFPSO
RMSE (mV)	21.4	11.6	8.99
MAE (mV)	16.8	6.95	4.56

Figure 4. The LIB terminals voltage absolute error by the CAFPSO PSO, AFPSO.

5. Conclusions

A new CAFPSO algorithm was derived to obtain accurate parameters' identification of LIBs models. A FIM was set up for modeling the LIB based on the EIS technique. A CAFPSO was then derived based on the logistic chaotic mapping method and used to initialize the particles' population in order to increase diversity. A speed updating law with adaptive FO was adopted to adjust the particle express delivery and position. The effectiveness of the CAFPSO was verified by comparing the LIB terminals voltage obtained with the parameters identified by the CAFPSO, the PSO and the AFPSO. Accuracy improvements of 22.5% and 34.4%, and 57.9% and 72.8%, in the RMSE and MAE, respectively, were obtained by the CAFPSO relative to the PSO and AFPSO. Future research will consider the temperature in the process of parameters' identification, since it was found that the accuracy of the FIM depends on this variable.

Author Contributions: Methodology, software, validation and data curation, writing—original draft preparation, writing—review and editing, supervision and project administration, D.W., H.W., J.X., F.W., A.M.L. All authors have read and agreed to the published version of the manuscript.

References

1. Huang, B.; Pan, Z.; Su, X.; An, L. Recycling of lithium-ion batteries: Recent advances and perspectives. *J. Power Sources* **2018**, *399*, 274–286. [CrossRef]
2. Xu, G.; Du, X.; Li, Z.; Zhang, X.; Zheng, M.; Miao, Y.; Gao, Y.; Liu, Q. Reliability design of battery management system for power battery. *Microelectron. Reliab.* **2018**, *88*, 1286–1292. [CrossRef]
3. Wang, Y.; Tian, J.; Sun, Z.; Wang, L.; Xu, R.; Li, M.; Chen, Z. A comprehensive review of battery modeling and state estimation approaches for advanced battery management systems. *Renew. Sustain. Energy Rev.* **2020**, *131*, 110015. [CrossRef]
4. Yang, R.; Xiong, R.; He, H.; Mu, H.; Wang, C. A novel method on estimating the degradation and state of charge of lithium-ion batteries used for electrical vehicles. *Appl. Energy* **2017**, *207*, 336–345. [CrossRef]
5. Hu, X.; Yuan, H.; Zou, C.; Li, Z.; Zhang, L. Co-estimation of state of charge and state of health for lithium-ion batteries based on fractional-order calculus. *IEEE Trans. Veh. Technol.* **2018**, *67*, 10319–10329. [CrossRef]
6. Xiong, R.; Tian, J.; Shen, W.; Sun, F. A novel fractional order model for state of charge estimation in lithium ion batteries. *IEEE Trans. Veh. Technol.* **2018**, *68*, 4130–4139. [CrossRef]

7. Sun, C.; Lin, H.; Cai, H.; Gao, M.; Zhu, C.; He, Z. Improved parameter identification and state-of-charge estimation for lithium-ion battery with fixed memory recursive least squares and sigma-point Kalman filter. *Electrochim. Acta* **2021**, *387*, 138501. [CrossRef]
8. Sun, Y.; Li, Y.; Yu, M.; Zhou, Z.; Zhang, Q.; Duan, B.; Shang, Y.; Zhang, C. Variable fractional order-a comprehensive evaluation indicator of lithium-ion batteries. *J. Power Sources* **2020**, *448*, 227411. [CrossRef]
9. Chen, L.; Wu, X.; Lopes, A.M.; Yin, L.; Li, P. Adaptive state-of-charge estimation of lithium-ion batteries based on square-root unscented Kalman filter. *Energy* **2022**, *252*, 123972. [CrossRef]
10. Chen, L.; Chen, Y.; Lopes, A.M.; Kong, H.; Wu, R. State of charge estimation of lithium-ion batteries based on fuzzy fractional-order unscented kalman filter. *Fractal Fract.* **2021**, *5*, 91. [CrossRef]
11. Chen, L.; Wu, X.; Tenreiro Machado, J.A.; Lopes, A.M.; Li, P.; Dong, X. State-of-charge estimation of Lithium-ion batteries based on fractional-order square-root unscented Kalman filter. *Fractal Fract.* **2022**, *6*, 52. [CrossRef]
12. Pang, H.; Mou, L.; Guo, L.; Zhang, F. Parameter identification and systematic validation of an enhanced single-particle model with aging degradation physics for Li-ion batteries. *Electrochim. Acta* **2019**, *307*, 474–487. [CrossRef]
13. Tian, N.; Wang, Y.; Chen, J.; Fang, H. One-shot parameter identification of the Thevenin's model for batteries: Methods and validation. *J. Energy Storage* **2020**, *29*, 101282. [CrossRef]
14. Kim, M.; Chun, H.; Kim, J.; Kim, K.; Yu, J.; Kim, T.; Han, S. Data-efficient parameter identification of electrochemical lithium-ion battery model using deep Bayesian harmony search. *Appl. Energy* **2019**, *254*, 113644. [CrossRef]
15. Lai, X.; Wang, S.; Ma, S.; Xie, J.; Zheng, Y. Parameter sensitivity analysis and simplification of equivalent circuit model for the state of charge of lithium-ion batteries. *Electrochim. Acta* **2020**, *330*, 135239. [CrossRef]
16. Wang, Z.; Feng, G.; Liu, X.; Gu, F.; Ball, A. A novel method of parameter identification and state of charge estimation for lithium-ion battery energy storage system. *J. Energy Storage* **2022**, *49*, 104124. [CrossRef]
17. Xu, Y.; Hu, M.; Zhou, A.; Li, Y.; Li, S.; Fu, C.; Gong, C. State of charge estimation for lithium-ion batteries based on adaptive dual Kalman filter. *Appl. Math. Model.* **2020**, *77*, 1255–1272. [CrossRef]
18. Yu, Z.; Huai, R.; Li, H. CPSO-Based Parameter-Identification Method for the Fractional-Order Modeling of Lithium-Ion Batteries. *IEEE Trans. Power Electron.* **2021**, *36*, 11109–11123. [CrossRef]
19. Kwak, M.; Lkhagvasuren, B.; Park, J.; You, J.H. Parameter identification and SOC estimation of a battery under the hysteresis effect. *IEEE Trans. Ind. Electron.* **2019**, *67*, 9758–9767. [CrossRef]
20. Li, L.; Wang, C.; Yan, S.; Zhao, W. A combination state of charge estimation method for ternary polymer lithium battery considering temperature influence. *J. Power Sources* **2021**, *484*, 229204. [CrossRef]
21. Jiang, C.; Wang, S.; Wu, B.; Fernandez, C.; Xiong, X.; Coffie-Ken, J. A state-of-charge estimation method of the power lithium-ion battery in complex conditions based on adaptive square root extended Kalman filter. *Energy* **2021**, *219*, 119603. [CrossRef]
22. Hua, X.; Zhang, C.; Offer, G. Finding a better fit for lithium ion batteries: A simple, novel, load dependent, modified equivalent circuit model and parameterization method. *J. Power Sources* **2021**, *484*, 229117. [CrossRef]
23. Podlubny, I. *Fractional Differential Equations, Mathematics in Science and Engineering*; Mathematics in Science and Engineering; Academic Press: San Diego, CA, USA, 1999; Volume 198.
24. Xu, J.; Mi, C.C.; Cao, B.; Cao, J. A new method to estimate the state of charge of lithium-ion batteries based on the battery impedance model. *J. Power Sources* **2013**, *233*, 277–284. [CrossRef]